Supplementary information

Two-dimensional Arrays Self-assembled *via* Interference of Concentration Modulation Waves in Drying Solution

Shunpu Li,‡[ab] Young Tea Chun,‡[a] Jin Li,[a] Pawan Shrestha,[a] Hyungju Ahn,[c] Docheon Ahn,[c] Jung Inn Sohn,[d] Woong-Ki Hong,[e] Bongjun Kim,[f] Yuanbo Deng,[a] and Daping Chu*[a]

（1）Preparation of samples with patterned structure. Most of the samples used in this work were made *via* liquid confinement in wedge geometry so that much stable liquid bridges could be formed with such geometry. For sample preparation, solutions were introduced using a micropipette into the wedge-shaped spaces formed with silicon substrates (12 mm × 12 mm) and glass cover plates (12 mm × 12 mm) with an angle of 25°. The joining of the substrate and cover plate can be made with epoxy. The substrates were treated with O_2 plasma (100 W for 5 min) to increase binding strength of the polymer pattern with substrate during deposition. For temperature-dependence experiments, before introduction of solutions with a micropipette, the assembled substrate/cover-plate wedges were placed on a digital hotplate and thermally stabilized for three minutes. Liquid confinement in parallel-plate geometry was done by introducing a solution into the space between substrates and parallel cover-plates (glass or PDMS) that were separated by spacers made of plastic films of various thicknesses. For obtaining micro-size separation, PDMS stamps with patterned trench arrays were used as top coverage.

（2）Estimation of the temperature dependence of spinodal-wavelength. We applied the viscosity values of toluene at room temperature and 60°C from reference (558 μPa.s for 24°C and 384 μPa.s for 60°C)[1] to equation (3) of this manuscript, and inserted it into the following expression:

$$\frac{\Delta\lambda}{\lambda} = \frac{\lambda(60\,℃) - \lambda(Room)}{\lambda(60\,℃)} \qquad (1)$$

We obtained $\Delta\lambda/\lambda$=19.46%, which was less than the data scattering of our experiments and this explains why no obvious temperature dependence was found in our experimental temperature range. This result also supported the validity of equation (3).

（3）Fabrication of arrays of deep sub-micrometre size. Fig.3D shows 2D P(NDI2OD-T2) pattern with deep sub-micrometre scale created by strong confinement of P(NDI2OD-T2) solution into micrometre thick thin film. Figure S5 shows a pattern-formation process of P(NDI2OD-T2) when its solution of 1,2-dichlorobenzene (or toluene, 5 mg/ml) was dried in a trench of a PDMS stamp. PDMS stamps with a patterned trench array (pattern size: 10 mm × 10 mm; single-trench dimension: length × width × height = 10 mm × 20 μm × 1.5 μm; trench separation: 20 μm) was duplicated from a photolithography-defined photo-resist pattern. Solution (3 μl) was dispensed on the stamp surface with a micropipette and dried against Si_2O/Si substrate with a small applied pressure (≈5 MPa) (Figure S5a). With solvent evaporation, the solution was split in the trench and liquid bridges were formed. Initially, no pattern was formed because the contact line was not pinned due to the capillary force. With the progression of drying, precipitation occurred, which might have been caused by crossing the binodal region of the solution composition (Figure S5b). Polymer precipitation induces a surface roughing and in turn a contact line pinning began. With further drying the solution concentration moves into the spinodal region. Eventually, patterned arrays were formed in the areas close to the walls of the trench (Figure S5c). Figure S5d shows an optical image of the polymer dried under the PDMS stamp with a patterned trench array.

（4）Relationship between the confined liquid-film thickness *h* and spinodal-wavelength λ_{sn}. For a first-order approximation, we assumed that a linear relationship was held between the spinodal-wavelength change and pressure change, $\Delta\lambda_{sn} = \chi\Delta p$ whereas, $\Delta\lambda_{sn} = \lambda_{sn} - \lambda_{sn}^{b}$, $\Delta P = -2\gamma\cos\vartheta/H$, and $H = h + \varepsilon$. Where χ is a constant; λ_{sn}^{b} is the spinodal-wavelength for a bulk liquid (i.e., thick solution film); γ, ϑ, H are surface tension (γ = 28.52 *mN/m* for toluene/air interface), contact angle ($\cos\vartheta \sim 1$ for well-wetted substrates), and effective thickness of the liquid film when the liquid/air interface is treated as a part of the cylinder surface; h is the real thickness of the liquid; ε is a constant in addition to h to calibrate the H value to remove the deviation of the meniscus shape from the ideal cylinder surface caused by substrate surface quality, mechanic vibration, and liquid gravity. Thus, we obtained:

$$\lambda_{sn} = \lambda_{sn}^{b} - \frac{2\chi\gamma\cos\vartheta}{h+\varepsilon} \qquad (2)$$

By choosing χ = 2.77×10^{-9}(m^3/N) and ε = 1.076×10^{-5}(m) the experimental λ_{sn}~h curve fitted nicely with equation (2) (red dotted line in Figure 3d).

(5) **Patterning on the tube surface.** It is possible to diversify the type of 2D lattices from rectangles by modifying the angle between the contact line and its moving direction. We demonstrated this with 2D-array generation on a glass tube surface. We loaded PMS toluene solution (5 wt %) into a space between a plastic cylinder container (internal diameter ϕ = 8.5 mm) and a glass tube to be patterned (ϕ = 6mm). When the glass tube was off-centred in the container with an appropriately adjusted gap between the container wall and the tube surface, a liquid hump could be formed via the capillary effect. When the solvent evaporated the contact line between the tube surface and liquid hump moved downwards, and a non-orthogonal relationship between the orientation of the contact line and its moving direction was created. Under this situation, the solute transport mechanism was also modified because gravity-induced convection plays an important role. In contrast, for the well-centred tube, the obtained PMS patterns had near-square symmetry. A 100 nm-thick Ge film was thermally evaporated on the tube surface to improve optical contrast for pattern examination.

(6) **Strain sensing.** We are able to obtain such 2D arrays with an area of several square millimetres, which is sufficiently large to demonstrate some functions. Figure 4c shows a diffraction pattern from a PMS array assembled from its toluene solution (5 mg/ml) with a He–Ne laser (beam size ϕ ≈1 mm) and a demonstration of strain sensing. Strain sensing was demonstrated on a 120 μm-thick polyethylene terephthalate (PET) film with a PMS pattern generated on it as a surface-labeled 2D grating. To increase light reflection, a 100-nm Ge film was thermally evaporated before generation of the PMS pattern using our method. Strain was created by bending a PET film (10 mm × 12 mm) with a homemade mechanic setup (Figure S6) while the displacement of first-order diffraction from zero-order diffraction was measured. Measurements were carried out with compression and tension states of the patterned surface (i.e., patterned surface in the concave/convex side). The increasing/decreasing of the displacement of the diffraction spots corresponded to decreased/increased lattice parameters during compression/tension of the patterned surface.

(7) **Modelled pattern surface profiles and pattern transfer.** The surface profile of the assembled patterns can be modeled by:

$$z = \frac{\xi}{2}\left(cos\frac{2\pi x}{\lambda_{sn}} + cos\frac{2\pi y}{\beta\lambda_{sn}}\right) \qquad (3)$$

where ξ is the distance between peak and valley and β is a constant which is close to one. Each peak is neighboured by four valleys and four saddle points (Figure S7a). This arrangement offers an advantage for pattern transferring. Positive and negative arrays can be generated from the same patterned film by control of dry etching. During pattern transfer, if the etching is stopped below the saddle points, a hole pattern will be defined (Figure S7b). A dot pattern will be obtained if the etching is stopped above the saddle points (Figure S7c). Figure S8 shows the pattern-transfer process we used. A 250 nm-thick polydimethylglutarimide (PMGI) layer was spin-coated on a Si substrate and baked for 30 min at 200°C, and then a 10 nm-thick Ge layer was thermally evaporated. A PMS polymer pattern was generated on the Ge layer using our method (Figure S8a). The patterned polymer was thinned by oxygen plasma to the desired thickness (below or above saddle points) (Figure S8b). Then, CF_4 plasma was used to etch through the Ge layer (Figure S8c). This was followed by oxygen plasma to etch through the PMGI using the thin Ge layer as an etching mask (Figure S8d). Finally, Au/Cr (30 nm/10 nm) films were deposited by thermal evaporation and a lift-off was done in a Microposit Remover (1165) (Figure S8e).

(8) **GIWAXD.** To gain information about hydrodynamic influence during solution drying under strong confinement, we undertook GIWAXD for the P(NDI2OD-T2) polymer dried in between a top PDMS plate and Si substrate with a separation of 1.5 μm. Sample preparation was identical to that for fabrication of the pattern with deep sub-micrometre size shown in Figure S5. GIWAXD was carried out at a PLS-II 9A U-SAXS beamline in the Pohang Accelerator Laboratory (Seoul, South Korea). Figure S9 shows the GIWAXD result from patterned P(NDI2OD-T2) samples (Figure S9a, S9b) and spin-coated film (Figure S9c), and a comparison of diffraction patterns (Figure S9d). Broad and weak peaks along the vertical axis (q_z) at q_z ≈1.55 Å^{-1} ($d_{\pi-\pi}$ = 4.05 Å) corresponded to a π-π stacking reflection for all samples (Figure S8a-c). The 2D GIWAXD image for the spin-coated film contained reflections from lamellar stacking (with the lowest order (100)) and chain-backbone-repeating (with the lowest order (001)) at q_{xy} = 0.246 Å^{-1} and 0.45 Å^{-1} along the in-plane direction. In addition, multiple diffraction peaks for the (n00) plane were observed along the out-of-plane direction. When the x-ray beam was aligned with the perpendicular direction to the patterned line, 2D GIWAXD images and the in-plane intensity profile only presented (n00) diffraction peaks, which were induced from face-on molecular packing. Otherwise, when the X-ray beam passed through the parallel direction with a line pattern, only reflection from chain-backbone repeating was observed.

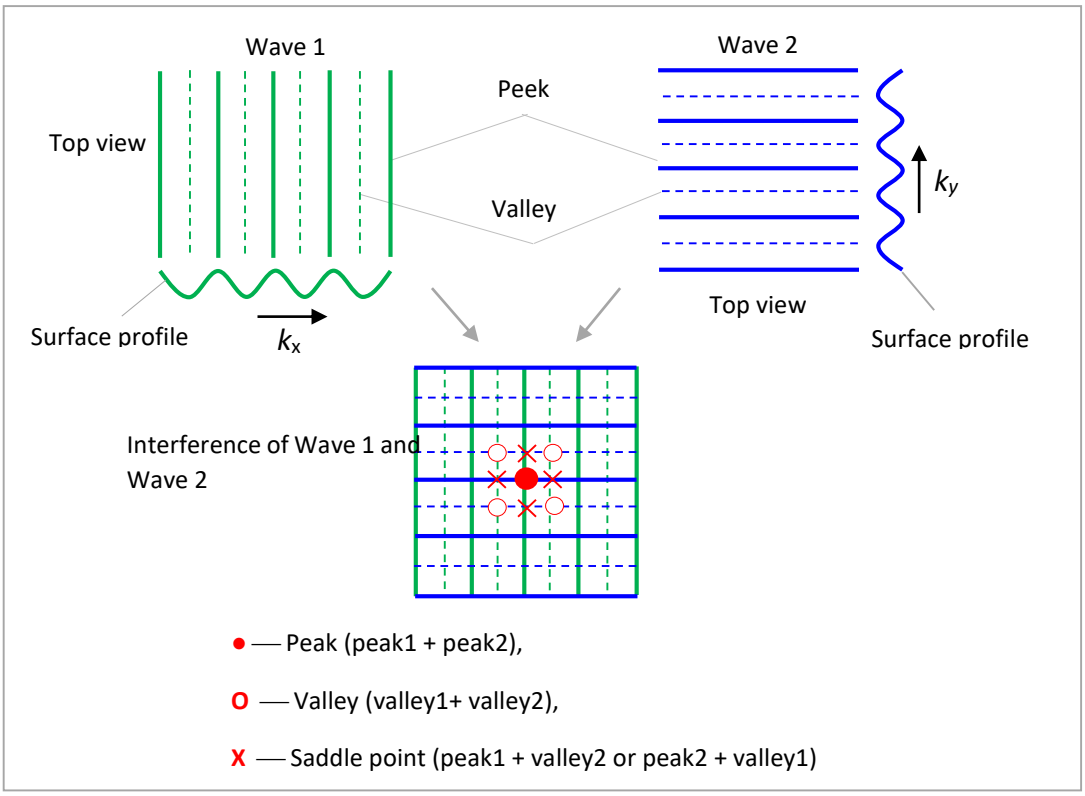

Figure S1. Interference of two orthogonal plane waves (schematic). The interference pattern of the two-waves can interpret the AFM result closely. Each peak (peak 1 + peak 2) is neighboured by four valleys (valley 1 + valley 2) and four saddle points (peak 1 + valley 2 and peak 2 + valley 1).

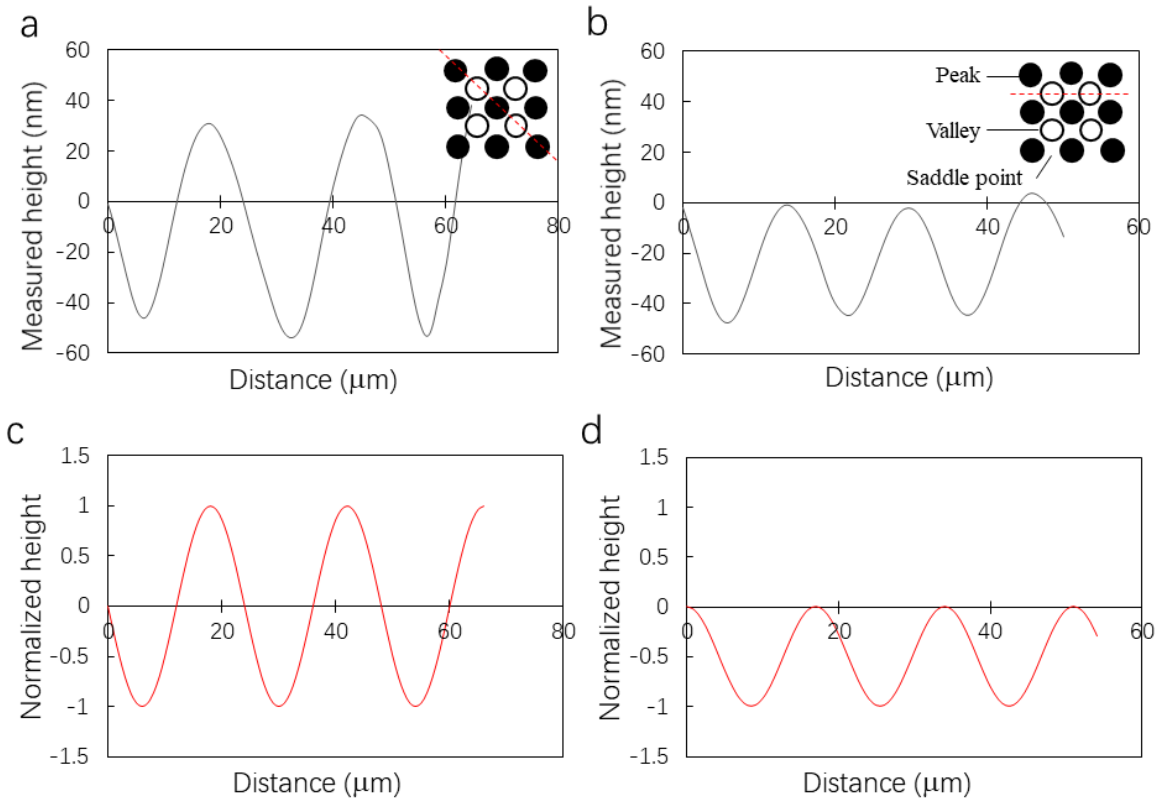

Figure S2. Comparison of AFM measurement (a, b)and modeled result(c, d). (a) Peak-Valley profile taken by scanning AFM tip through diagonal direction (red doted line of inset) of an assembled PMS square array and its modeled result is shown in (c). (b) Saddle-Valley profile taken by scanning AFM tip along the contact line direction (red doted line of inset) and its modelling result is shown in (d). Because the starting point of the AFM measurement was arbitrarily chosen a phase shift was added in the equation (1) of the manuscript for a clear comparison between the modelling and experiment. For the modelling a measured value of λ_{sn} =17μm was used.

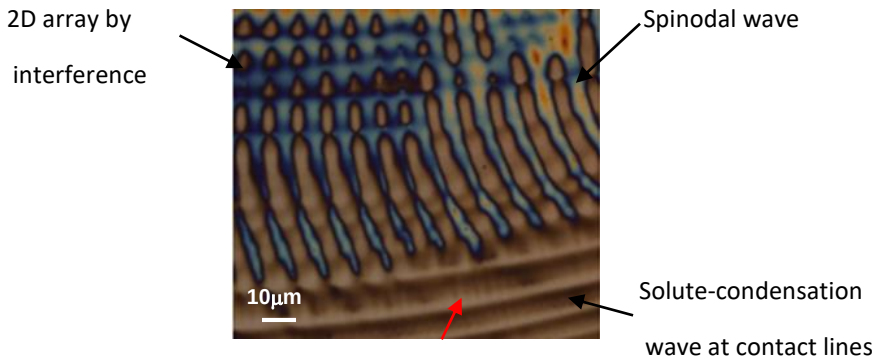

Figure S3. The optical image of a PVP structure dried from IPA solution (5mg/ml). Three regions are shown, which were caused by fluctuations of wave amplitude. When the spinodal (SN) wave amplitude is dominant over the solute-condensation (SC) wave, a line array that is perpendicular to the contact line is obtained. In contrast, if the SC-wave is dominant, a line array that is parallel to the contact line is obtained. If the amplitudes of the two waves are balanced a 2D array is formed. A shorter-wavelength mode of the SN wave can also be seen (red arrow).

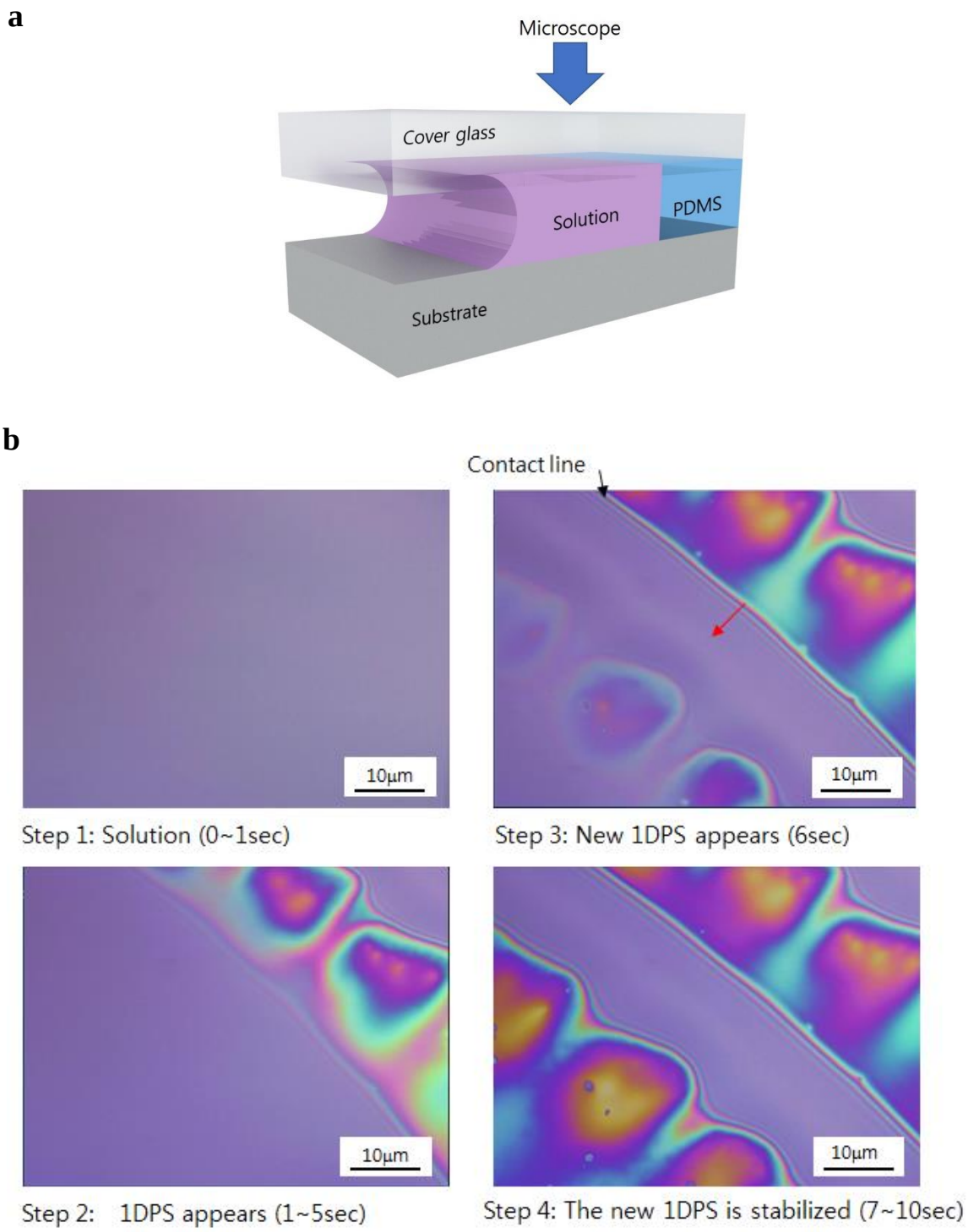

Figure S4. *In situ* observation of the formation of a PMS polymer pattern. (a) Schematic illustration of the experimental setup we used, where the PDMS film was used as a spacer to separate the substrate and cover glass. (b) Sequence images selected from a supporting video (red arrow indicates the moving direction of the contact line).

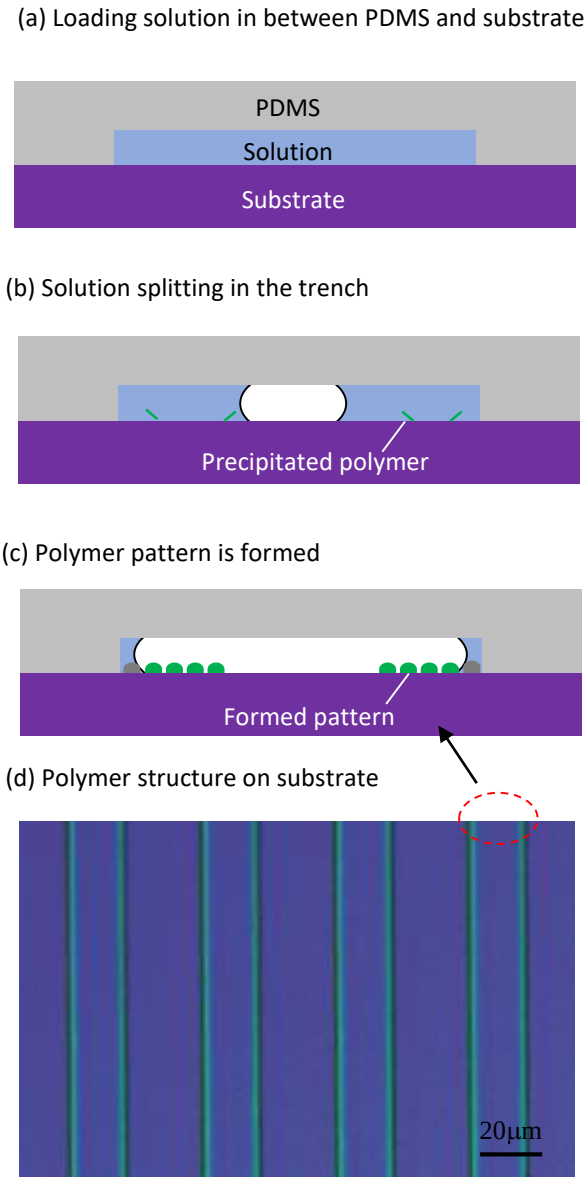

Figure S5. Schematic illustration of formation of polymer pattern with deep sub-micrometre resolution and experimentally generated polymer structure on the substrate. (a–c) Process of pattern formation. (d) The polymer structure formed under a line-patterned PDMS.

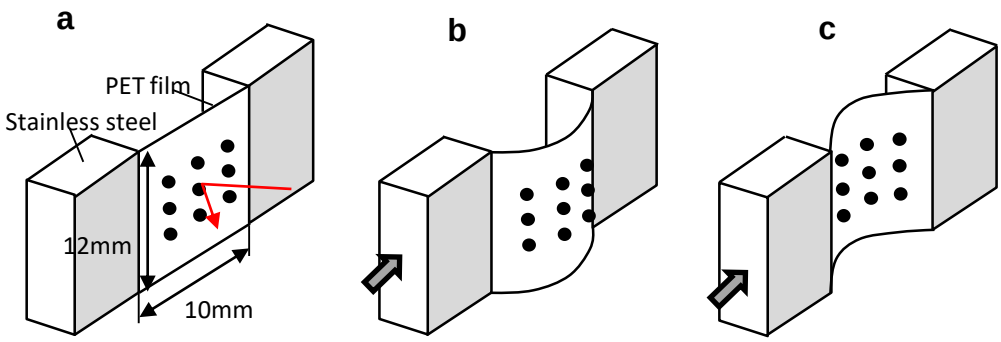

Figure S6. Schematic illustration of film bending for a strain sensing experiment. The three experimental conditions are the strain-free state of the film (a), patterned surface under tension strain (b), and patterned surface under compression strain(c), respectively. Strain sensing was done using a homemade clamp consisting of two stainless-steel parts and their distance could be precisely tuned. A PET film (10 mm × 12 mm) with a PMS pattern on it was fixed between the two parts with Scotch™ tape and bending was done by tuning the distance of the two parts.

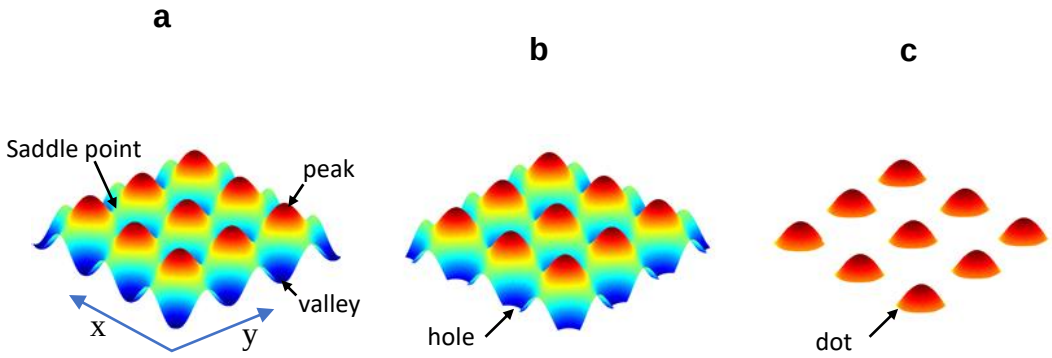

Figure S7. Modeled surface profiles before and after plasma etching. (a) General surface profile of the pattern modeled. (b) A hole pattern was obtained when plasma etching was stopped below saddle points. (c) A dot pattern was defined if the etching was stopped above the saddle points.

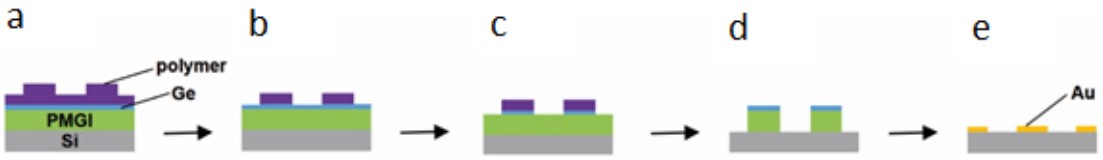

Figure S8. Pattern-transfer process used in this work to transfer PMS patterns to Au structures. (a) Pattern formation. (b) O_2 plasma etching. (c) CF4 plasma etching. (d) O_2 plasma etching. (e) Lift-off.

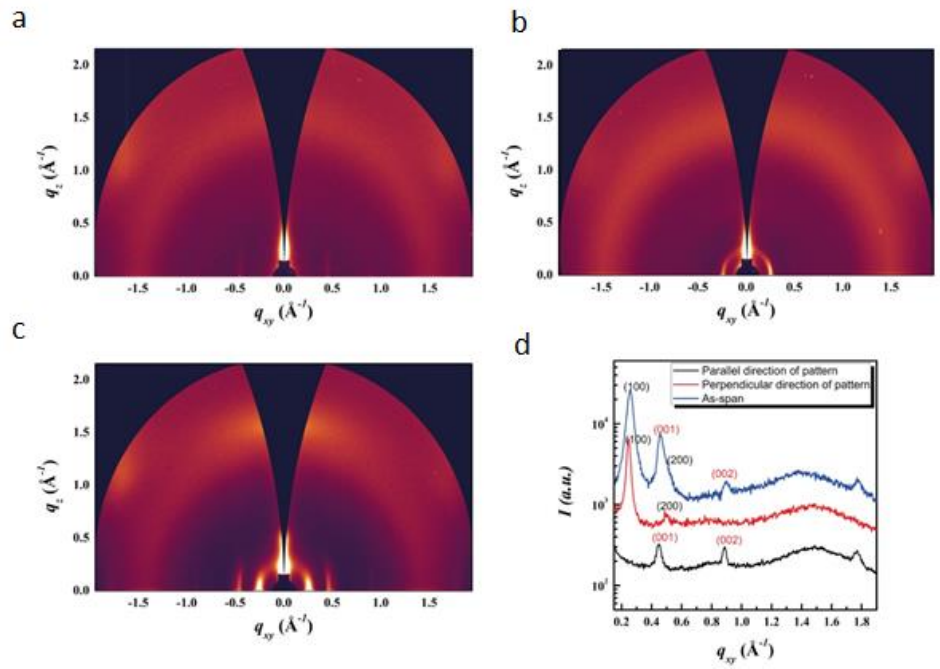

Figure S9. GIWAXD measurement under various conditions. (a) Beam orientation is along the direction of pattered lines (i.e., the trench direction). (b) Beam orientation is perpendicular to patterned lines. (c) Result of a spin-coated film. (d) Comparison of diffraction patterns taken with various conditions.

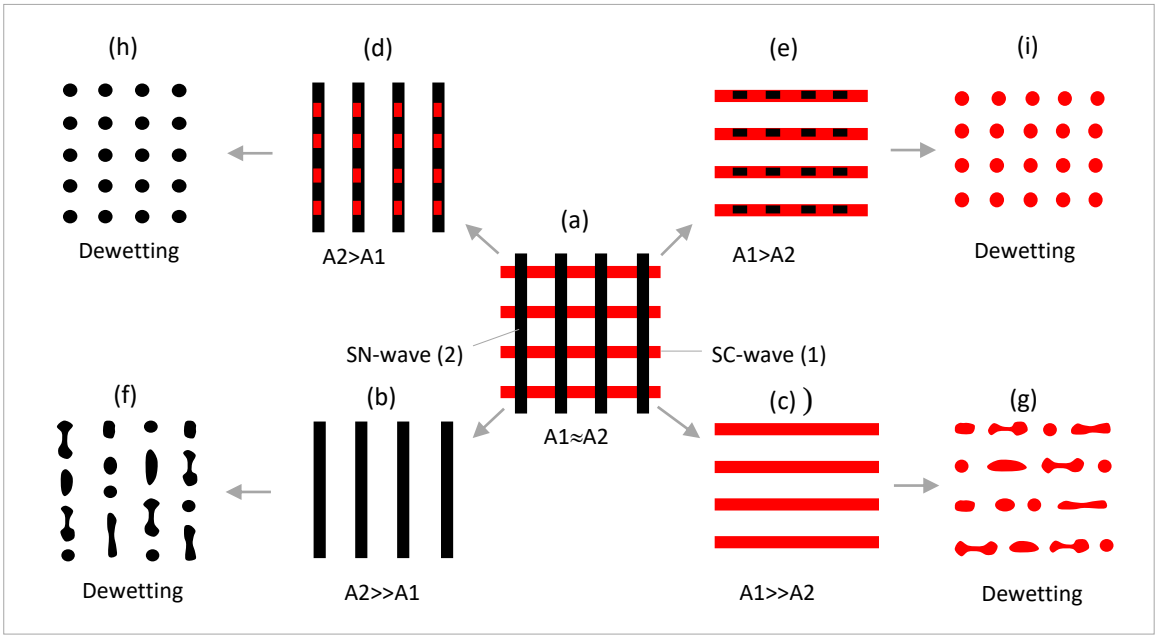

Figure S10. Summary of patterns that may be observed by drying solution under different conditions. When the amplitudes of both waves (A1, A2) are well balanced, a normal interference pattern with potential high resolution can be observed (a). Four types of line patterns may exist depending on the degree of misbalance of amplitudes of the two waves. If the SN-wave (SC-wave) is absolutely dominant over the SC-wave (SN-wave), then normal arrays of lines perpendicular (parallel) to the contact line can be obtained (b, c). If they are partially dominant over the amplitudes of their counterpart waves, then the patterned lines are modulated (with composition/film-thickness/line-width) (d, e). If dewetting occurs, the normal line patterns produce irregular dot pattern (f, g), whereas the modulated line patterns produce ordered dot arrays (h, i).

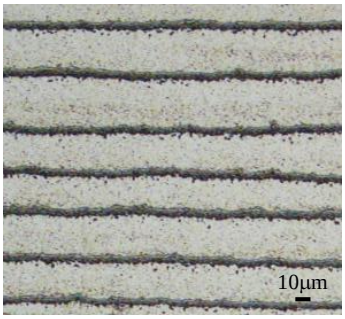

Figure S11. ZnO line pattern fabricated by drying ZnO particle (100nm in diameter) suspension in ethanol (5mg/ml). The patterned lines are less regular and no spinodal process is found.